Computational Materials Science 50 (2011) 3425–3430: doi:10.1016/j.commatsci.2011.07.004

Numerical exploration of plastic deformation mechanisms of copper nanowires with surface defects

H.F. Zhan[1], Y.T. Gu[1*], C. Yan[1], X.Q. Feng[2], and P. K.D.V. Yarlagadda[1]

[1]*School of Engineering Systems, Queensland University of Technology, Brisbane, 4001, Australia*

[2]*Department of Engineering Mechanics, Applied Mechanics Laboratory, Tsinghua University, Beijing 100084, China*

***Corresponding author:** Dr. Yuantong Gu

Mailing Address: School of Engineering Systems,

Queensland University of Technology,

GPO Box 2434, Brisbane, QLD 4001, Australia

Telephones: +61-7-31381009

Fax: +61-7-31381469

E-mail: yuantong.gu@qut.edu.au

Computational Materials Science 50 (2011) 3425–3430: doi:10.1016/j.commatsci.2011.07.004

Abstract

Based on the molecular dynamics simulation, plastic deformation mechanisms associated with the zigzag stress curves in perfect and surface defected copper nanowires under uniaxial tension are studied. In our previous study, it has found that the surface defect exerts larger influence than the centro-plane defect, and the 45^o surface defect appears as the most influential surface defect. Hence, in this paper, the nanowire with a 45^o surface defect is chosen to investigate the defect's effect to the plastic deformation mechanism of nanowires. We find that during the plastic deformation of both perfect and defected nanowires, decrease regions of the stress curve are accompanied with stacking faults generation and migration activities, but during stress increase, the structure of the nanowire appears almost unchanged. We also observe that surface defects have obvious influence on the nanowire's plastic deformation mechanisms. In particular, only two sets of slip planes are found to be active and twins are also observed in the defected nanowire.

Keywords: plastic deformation mechanism, defect, nanowire, tension, molecular dynamics

1. Introduction

Nanowires are attracting considerable technological interest due to their immense applications that arise from their unique mechanical, electrical, optical and other properties [1, 2]. They have been utilized as ultrahigh-resolution mass sensors, nanowire circuits, nanowire field-effect transistors, tips for the scanning force and tunnelling microscope (STM), and other devices [3-5]. Recently, many researchers proposed the nanowires' usage in the solar energy conversion devices to make the solar energy cheaper and with higher efficient than the current technology [6]. Therefore, a fundamental understanding of nanowires' characteristics is increasingly required. Numerous experimental studies have been conducted. For example, Wu employed [7] the atomic force microscope (AFM)-based bending experiments to measure the mechanical properties (Young's modulus and yield strength) of Au nanowires. The AFM-based nanoindentation experiments were carried out by Ni et al. [8] to measure the Young's modulus of ZnO nanobelts. Dikin et al. [9] reported the resonance vibration studies of SiO_2 nanowires driven by mechanical or electrical field excitations. Recently, Marszalek et al. [10] demonstrated that experiments can provide direct evidence for the mechanism underlying the plastic deformation of a nanowire, based on the measurement of the length of Au nanowire structure during extension and compression cycles.

In despite of the inspiring results obtained from experimental studies, controlling experimental test conditions at the nanoscale is supposed facing with inherent complexities and unknowns, which has led to extensive employments of numerical approaches [11, 12]. Furthermore, numerical approaches could provide insights of the

deformation progress, which is lack in traditional experimental studies. Such insights can also greatly benefit the fundamental understanding of deformation mechanisms of nanomaterials. Extensive numerical studies have been dedicated to explore the mechanical behaviour of metallic nanowires, including the Cu, Al, Ag and Au nanowires [13-15], e.g. studies of mechanical responses of metal nanowire under the deformation of torsion [16] and bending [17, 18], and also the buckling phenomenon [19, 20] have been reported. Recently, it is found that surfaces exert great influences on the structure and properties of nanowires, the surface Cauchy-Born approach was proposed by Park et al. [21, 22] to model FCC metals with nanoscale dimensions to address the surface's significant effect to the overall mechanical response. Researchers have reported the surface-stress-induced phase transformation [23], pseudoelastic behaviour [24] and a novel memory effect [25, 26] in nanowires, which are believed originating from the nanowires' significant surface-to-volume ratio.

Due to the ease of the tensile stress analysis in an atomistic framework, numerical studies of nanowires subjected to the uniaxial tension have been frequently conducted. Generally, a saw-toothed [27, 28] or a zigzag [29] stress curve during the plastic deformation has been reported in most publications relating to the nanowires' tensile deformation. However, previous numerical studies were mostly focused on the prediction of material properties such as the Young's modulus and yielding strength [30, 31]. It still lacks a comprehensive understanding of the mechanism for formation of these zigzag stress curves. Therefore, in this research, an in-depth numerical study of the deformation mechanism of the zigzag stress curve will be conducted. Furthermore, most existing numerical studies mainly focused on perfect nanowires. In fact, materials are usually not perfect, that is, defects are always unavoidable such as impurities, grain boundaries, surface defects, nano-cavities and others. In our previous study [32], we systematically investigated the effects of different surface and centro-plane defects on the general mechanical properties (like Young's modulus and yield strength) of nanowires during tensile deformation, major findings were as follows:

- The Young's modulus is found insensitive to different styles of defects, however, the yield strength and yield strain appear a large decrease due to different defects.
- Defects have played a role of dislocation sources, slips or SFs are first generated around the locations of defects. Necking locations have also been affected due to different defects.
- Generally, the surface defect induces bigger decrease to the yield strength than the centro-plane defect, and the 45º defect induces the largest influence in all orientations.

As our previous work is focusing on the discussion of the defect's influence to the general mechanical properties, to obtain a comprehensive understanding of defects' effects, an in-depth investigation of the plastic deformation mechanism is required. Therefore, according to aforementioned findings, in this work, the defect's effect to the plastic deformation mechanism of the nanowire with a 45º surface defect will be carefully investigated.

2. Numerical implementation

Molecular dynamics (MD) simulations are carried out on copper nanowires subjected to tensile deformation. The Large-scale Atomic/Molecular Massively Parallel simulator (LAMMPS) [33] is employed to carry out the MD simulation. The square cross-section copper nanowire with the initial atomic configuration positioned at the FCC lattice site is considered, and the x, y, z coordinate axes represent the lattice direction of [100], [010], [001], respectively. Two different cases with the same size have been considered, as shown in Figure 1, including a perfect nanowire and a nanowire with a 45º surface defect. The size of the specimen is chosen as $2.166\text{nm}\times 2.166\text{nm}\times 15.88\text{nm}$. The defected nanowire is obtained by removing several atoms on the (100) surface, and introducing a 45° surface defect. Nanowires are first relaxed to a minimum energy state using the conjugate gradient energy minimization and then the Nose-Hoover thermostat [34, 35] is employed to equilibrate the nanowires at 0.01K. After that, a constant strain rate is applied in the z direction. No periodic boundary condition is adopted.

The following embedded-atom-method (EAM) potential [36, 37] as developed for copper by Mishin [38] is used to describe the atomic interactions in these simulations.

$$E_{tot} = \sum_i F(\rho_i) + \frac{1}{2}\sum_i \sum_j V(r_{ij}) \ , \rho_i = \sum_j \Phi(r_{ij}) \tag{1}$$

here V , F , ρ are the pair potential, the embedded energy, and the electron cloud density, respectively. i , j are the number of atoms, and r_{ij} is the distance between them. This potential is chosen as it can reliably predict the material stacking faults energies and the stability of nonequilibrium structures of copper. The equations of motion are integrated with time using a Velocity Verlet algorithm [39].

In order to analyse the partial dislocation and stacking faults (SFs) during the tensile deformation, the centro-symmetry parameter [40] (csp) is used, which is defined as follows:

$$csp = \sum_{i=1,6} \left| \vec{R}_i + \vec{R}_{i+6} \right|^2 \tag{2}$$

where $\vec{R}_i$ and $\vec{R}_{i+6}$ are vectors corresponding to the six pairs of opposite nearest neighbours in FCC lattice. The csp value increases from 0 for perfect FCC lattice to positive values for defects and for atoms close to free surfaces. In this work, $0.5 < csp \le 3$, $3 < csp \le 12$, and $csp > 12$ are assigned to identify the partial dislocations, SFs and surface atoms, respectively. According to the csp value, intrinsic SFs will have two adjacent SFs layers and for extrinsic SFs or twins, only two translated SFs layers will be observed with atoms between the top and bottom layers still in the FCC environment. For convenience, we employ the following denotations as, t: the time,

unit ps; σ: the stress, unit GPa; ε : the strain; Np : the number of partial dislocations atoms; Ns : the number of SFs atoms; N : the total number of the dislocation atoms, where $N = Np + Ns$.

3. Deformation mechanism analysis

The $\sigma - \varepsilon$ curves of the perfect and surface defected nanowires under uniaxial tension are plotted in Figure 2. As reported by other researchers, the stress is found increased approximately linearly in the elastic deformation region for the perfect nanowire. During the plastic deformation region, the stress shows the saw-toothed or zigzag changing tendency. Similar $\sigma - \varepsilon$ curve's schematic is also found for the surface defected nanowire. The analysis of deformation mechanisms behind such zigzag stress curve is carried out in the following section. The atomic configurations at different times are selected to best clarify the deformation process of nanowires.

3.1 Perfect nanowire analysis

The $\sigma - t$, $N - t$, $Ns - t$ and $Np - t$ curves of the perfect nanowire under uniaxial tension are presented in Figure 3. As the structure of the nanowire remains basically unchanged during the elastic deformation, and values of Np and Ns are zero, only curves within the plastic deformation region are provided. Generally, according to Figure 3(a), we find a zigzag $\sigma - t$ curve and a staircase-shaped $N - t$ curve after yielding. A clear correlation is found between σ and N , which is similar as the relationship between the force and the conductance reported by Sorensen et al. [41], when they investigated the mechanical deformation of atomic-scale metallic contacts. To explore the deformation mechanism underlying the zigzag stress curve, major inflexion events are identified (label 1-13), dividing the stress curve into two types of regions including stress increase regions (e.g. 2-3) and stress decrease regions (e.g. 1-2). From Figure 3(b), the value of Ns is found fluctuated around 1600 during the whole plastic deformation process, but a much smaller value around 40 is found for Np . This large gap makes N and Ns curves share almost the same changing tendency, therefore, the following discussion will focus on $Ns - t$, $Np - t$ and $\sigma - t$ curves. In-depth investigations of atomic configurations suggest that, stress decrease regions are always accompanied with activities of SFs generation and migration but the structure of the entire nanowire appears almost unchanged in stress increase regions.

Specifically, for stress decrease regions (like regions 1-2, 3-4, and others), Ns appears fluctuations. Two situations have contributed to these fluctuations. One is the generation of new SFs, which will increase the value of Ns, such as region 1-2. Another is when there are only SFs movements happened, Ns should be almost the same as previous value. Particularly, the SFs generation process is found to propagate the entire nanowire during region 1-2. Such special deformation region is referred as the first stage of plastic deformation in the following context. According to Figure 4(a), the SFs are observed occurring in all four different sets of {111} planes, with the existence of both intrinsic SFs α and extrinsic SFs β . The abundance activities of SFs in region 1-2 result in

a sharp increase of Ns, as shown in Figure 3(b). In fact, the $Ns-t$ curve doesn't increase smoothly in this region, several decrease events have been detected, and an obvious one is pointed out in Figure 3(b). We find that these decrease events are produced by the annihilation of intrinsic SFs. In other words, the perfect $\{111\}<100>$ dislocation is accomplished by glides of two partial dislocations that occur on the same {111} plane. Further, in regions 5-6, 7-8 and 11-12, an obvious decrease of Ns is found. These decrease phenomena are achieved by two kinds of mechanisms. The first is because of the aforementioned generation of perfect dislocation. The second is because of surface steps, some part of the SFs layers changed into surface, which eventually induces a decrease of SFs atoms Ns, as illustrated in Figure 4(d). For stress increase regions (e.g., regions 4-5, 6-7, and others), Ns is fairly constant. One exception is found in region 2-3, during which an obvious step increase is pointed out in Figure 3(b). According to Figure 4(b), the generation of new intrinsic SFs γ is found related to this event. The fixed end condition stopped its further generation, which eventually prevents this activity resulting in an obvious stress decrease.

The transition process from an intrinsic SFs to an extrinsic SFs is illustrated in Figure 5. Apparently, due to the rhombus shape of the slip plane, Np will increase once the partial dislocation nucleated, and get its peak value when the propagation arrives the middle of the slip plane, then decrease with further propagation. As the value of Np is very small, it make Np very sensitive to its variation. Clearly, the above procedure composes of a spike event to the Np value. Similar phenomena should also be obtained from the generation of an intrinsic SFs or twins. Therefore, spike events in the $Np-t$ curve during stress decrease regions are signs of partial dislocations nucleation and propagation activities. In the other hand, the relative smooth change of Np during stress increase regions can also be explained. In the first circumstance, for the preparation of the generation of new intrinsic SFs, extrinsic SFs or twins, Np will receive a smooth increase (like region 2-3). In the second circumstance, if a previous unaccomplished movement of partial dislocation is going to receive further propagation (see Figure 5(b)), then Np will appear as undulated (like region 4-5 and 6-7). The above explanations are well approved by atomic configurations. In all, the complete or uncompleted processes of the nucleation and propagation of partial dislocations are well reflected by the $Np-t$ curve.

Generally, we find that, stress decrease events are accompanied by the nucleation and propagation of partial dislocations, but during stress increase periods, the structure of the nanowire remains unchanged. It is observed that, most of the SFs are generated at the first stage of plastic deformation, and after this stage, most of the activities of partial dislocations are concentrated around the necking area, as shown in Figure 4(c).

3.2 Nanowire with surface defect analysis

The $\sigma - t$, $N - t$, $Ns - t$ and $Np - t$ curves of the defected nanowire during the plastic deformation are shown in Figure 6. Similar as the perfect nanowire, we find a zigzag $\sigma - t$ curve and also a staircase-shaped $N - t$ curve. The relationship between σ and N is highly consistent with that of perfect nanowire. Certain similarities of the deformation process between these two cases are observed. For example, after the first stage of plastic deformation (region A), most deformation activities are concentrated around the necking area. During stress increase regions, the structure of the nanowire appears almost unchanged (regions C and D), followed by a almost constant value of N, and stress decrease regions are accompanied with the generation and migration activities of SFs (regions A, B and E).

Besides the above similarities, different deformation mechanisms have been identified. Firstly, comparing with 279 ps duration of the first stage of plastic deformation for the perfect nanowire, a shorter duration about 130 ps is found for the defected nanowire. The quicker completion of the first stage of plastic deformation suggests that the defect makes dislocations easier to happen. More specifically, for the defected nanowire, the SFs are only produced in the $(\bar{1}1\bar{1})$ and $(11\bar{1})$ slip planes, as shown in Figure 7(a). We believe that, as the surface defect lies in the [110] direction, which is the common side of the $(\bar{1}1\bar{1})$ and $(11\bar{1})$ slip planes, therefore, only these two slip planes have been activated. Secondly, for the perfect nanowire under tension, the plastic deformation was reported to be dominated by slips [42, 43], which is also well illustrated in Figure 4. However, for the defected nanowire, we find the major plastic deformation is the transition between extrinsic SFs and twins. According to Figure 7(b), we observe the structure of extrinsic SFs at the time of 4388 ps transforms into the twins' structure with further elongation at the time of 4432 ps. Thirdly, we find the formation of three adjacent SFs layers around the necking area at the time of 5068 ps, as shown in Figure 7(c), which indicates the generation of the HCP structure. However, such HCP structure does not last for a long time. As seen in Figure 7(c), at the time of 5166 ps, the HCP structure turns into a twins' structure. This deformation process from HCP structure to twins is well tracked by the adjacent step increase and decrease events in the $Ns - t$ curve, as pointed out in Figure 6(b). It is worth to mention that, during this deformation process, two corresponding spike events are found in the $Np - t$ curve, as marked out in Figure 6(b). In addition, comparing with Figure 4(d) and 7(d), the necking phenomenon of the perfect and defected nanowire are also found different. The necking area is found located around the middle for the defected nanowire, but away from the middle for the perfect nanowire.

4. Conclusions

In summary, based on the molecular dynamics simulation, plastic deformation mechanisms behind the zigzag stress curves of the perfect and surface defected nanowires have been studied. With the analysis of atomic

configurations, the numbers of the partial dislocation atoms and SFs atoms have been employed to analyse the zigzag stress curves. The following conclusions have been drawn:

(1). During the plastic deformation, stress decrease regions are always accompanied with the SFs' generation and migration activities, but the structure of the nanowires remains almost unchanged within stress increase regions.

(2). Obvious influence on the deformation mechanism from surface defects has been observed. In particular, only two sets of slip planes are found to be active and twins are observed in the defected nanowire.

(3). For both perfect and defected nanowires, the generation of intrinsic SFs and extrinsic SFs have been observed and the deformation activities are concentrated around the necking area after the first stage of plastic deformation.

This study provides a fundamental understanding of the deformation mechanism of the nanowire under tension and also demonstrates the influence of surface defects on the plastic deformation.

References

[1] Y. Xia, P. Yang, Y. Sun, Y. Wu, B. Mayers, B. Gates, Y. Yin, F. Kim, H. Yan, Adv. Mater., 15 (2003) 353-389.

[2] J. Sarkar, G. Khan, A. Basumallick, Bull. Mater. Sci., 30 (2007) 271-290.

[3] Y. Yang, C. Callegari, X. Feng, K. Ekinci, M. Roukes, Nano Lett., 6 (2006) 583-586.

[4] N.A. Melosh, A. Boukai, F. Diana, B. Gerardot, A. Badolato, P.M. Petroff, J.R. Heath, Science, 300 (2003) 112.

[5] X. Duan, Y. Huang, C.M. Lieber, Nano Lett., 2 (2002) 487-490.

[6] A. Christ, T. Zentgraf, J. Kuhl, S. Tikhodeev, N. Gippius, H. Giessen, Phys. Rev. B, 70 (2004) 125113.

[7] B. Wu, A. Heidelberg, J.J. Boland, Nat. Mater., 4 (2005) 525-529.

[8] H. Ni, X. Li, Nanotechnology, 17 (2006) 3591.

[9] D. Dikin, X. Chen, W. Ding, G. Wagner, R. Ruoff, J. Appl. Phys., 93 (2003) 226.

[10] P.E. Marszalek, W.J. Greenleaf, H. Li, A.F. Oberhauser, J.M. Fernandez, Proc. Natl. Acad. Sci., 97 (2000) 6282.

[11] M. McDowell, A. Leach, K. Gall, Modell. Simul. Mater. Sci. Eng., 16 (2008) 045003.

[12] H.S. Park, W. Cai, H.D. Espinosa, H. Huang, MRS Bull., 34 (2009) 178-183.

[13] Y.G. Zheng, H.W. Zhang, Z. Chen, C. Lu, Y.W. Mai, Phys. Lett. A, 373 (2009) 570-574.

[14] K. Gall, J. Diao, M.L. Dunn, Nano Lett., 4 (2004) 2431-2436.

[15] H.S. Park, J.A. Zimmerman, Scripta Mater., 54 (2006) 1127-1132.

[16] S. Jiang, H. Zhang, Y. Zheng, Z. Chen, J. Phys. D: Appl. Phys., 42 (2009) 135408.

[17] J. He, C.M. Lilley, Nano Lett., 8 (2008) 1798-1802.

[18] G. Wang, X. Feng, Appl. Phys. Lett., 94 (2009) 141913.

[19] P.A.T. Olsson, H.S. Park, Acta Mater., (2011).

[20] W. Jiang, R. Batra, Acta Mater., 57 (2009) 4921-4932.

[21] H. Park, P. Klein, Phys. Rev. B, 75 (2007) 85408.

[22] H. Park, P. Klein, G. Wagner, Int. J. Numer. Meth. Engng, 68 (2006) 1072-1095.

[23] H.S. Park, Nano Lett., 6 (2006) 958-962.

[24] W. Liang, M. Zhou, F. Ke, Nano Lett., 5 (2005) 2039-2043.

[25] H.S. Park, K. Gall, J.A. Zimmerman, Phys. Rev. Lett., 95 (2005) 255504.

[26] H.S. Park, C. Ji, Acta Mater., 54 (2006) 2645-2654.

[27] H.A. Wu, Eur. J. Mech. - A/Solids, 25 (2006) 370-377.

[28] W. Liang, M. Zhou, Nanotechnology, 2 (2003) 452-455.

[29] L. Yuan, D. Shan, B. Guo, J. Mater. Process. Technol., 184 (2007) 1-5.

[30] M. McDowell, A. Leach, K. Gall, Nano Lett., 8 (2008) 3613-3618.

[31] A. Koh, H. Lee, Nano Lett., 6 (2006) 2260-2267.

[32] H.F. Zhan, Y.T. Gu, P.K.D.V. Yarlagadda, Adv. Sci. Lett., (2011 In press).

[33] S. Plimpton, P. Crozier, A. Thompson, Sandia National Lab, (2007).

[34] W.G. Hoover, Phys. Rev. A, 31 (1985) 1695-1697.

[35] S. Nosé, J. Chem. Phys., 81 (1984) 511.

[36] S. Foiles, M. Baskes, M. Daw, Phys. Rev. B, 33 (1986) 7983-7991.

[37] M. Daw, M. Baskes, Phys. Rev. B, 29 (1984) 6443-6453.

[38] Y. Mishin, M. Mehl, D. Papaconstantopoulos, A. Voter, J. Kress, Phys. Rev. B, 63 (2001) 224106.

[39] S. Plimpton, J. Comput. Phys., 117 (1995) 1-19.

[40] C. Kelchner, S. Plimpton, J. Hamilton, Phys. Rev. B, 58 (1998) 11085-11088.

[41] M.R. Sørensen, M. Brandbyge, K.W. Jacobsen, Phys. Rev. B, 57 (1998) 3283-3294.

[42] H. Park, K. Gall, J. Zimmerman, J. Mech. Phys. Solids, 54 (2006) 1862-1881.

[43] J. Diao, K. Gall, M. Dunn, J. Zimmerman, Acta Mater., 54 (2006) 643-653.

Computational Materials Science 50 (2011) 3425–3430: doi:10.1016/j.commatsci.2011.07.004

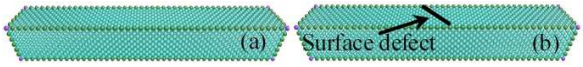

Figure 1. Simulation models: (a) Perfect nanowire; (b) Nanowire with 45° surface defect.

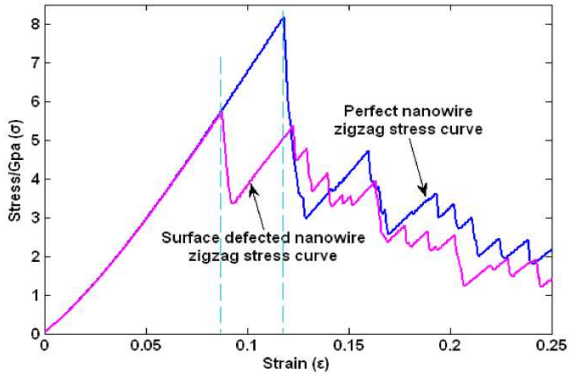

Figure 2. Stress-strain curve of the perfect and surface defected nanowires.

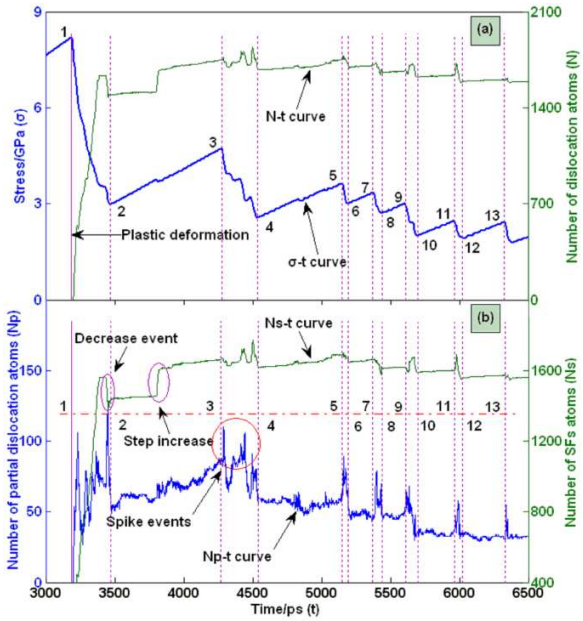

Figure 3. Perfect nanowire: (a) Stress and the number of dislocation atoms versus time; (b) Number of partial dislocations atoms and SFs atoms versus time.

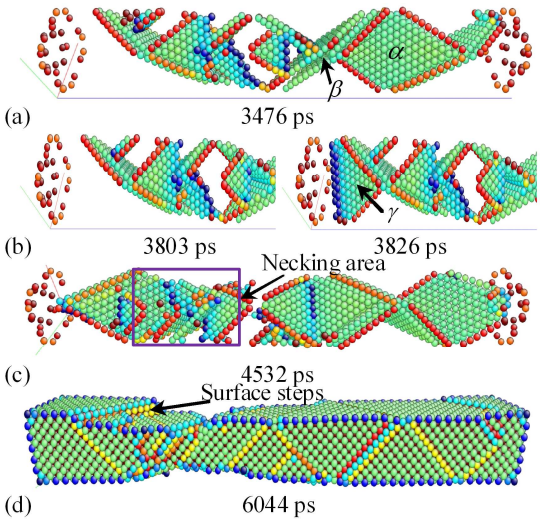

Figure 4. Atomic configurations of the perfect nanowire: (a) After the first stage of plastic deformation; (b) Intrinsic SFs generation; (c) Necking area; (d) Surface steps generation. In Figure (d), atoms with the coordination number between 4~12 are viewed. Other figures, atoms with the *csp* value between 0.5~12 are viewed.

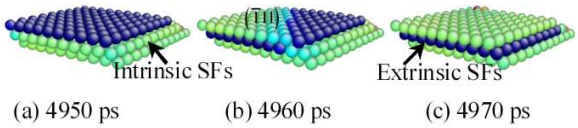

Figure 5. Transition from an intrinsic SFs to an extrinsic SFs. (a) Intrinsic SFs; (b) Half transformed intrinsic SFs; (c) Extrinsic SFs. Atoms with the *csp* value between 0~12 are viewed.

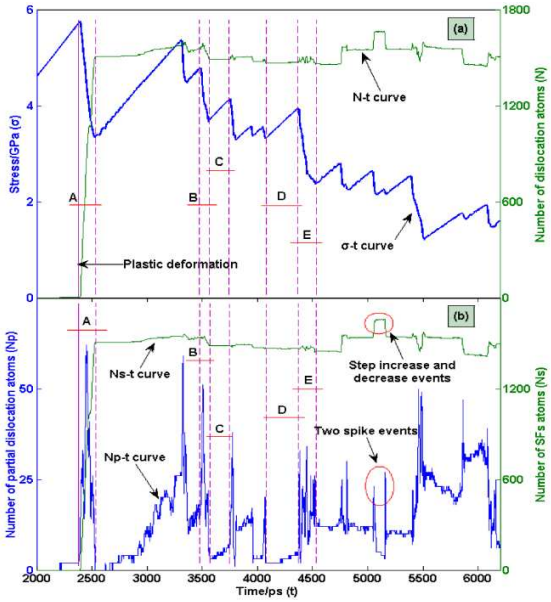

Figure 6. Defected nanowire: (a) Stress and the number of dislocation atoms versus time; (b) Number of partial dislocations atoms and SFs atoms versus time.

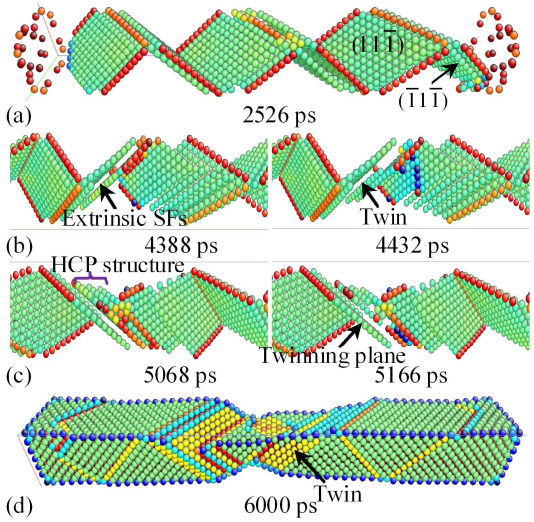

Figure 7. Atomic configurations of the defected nanowire: (a) After the first stage of plastic deformation; (b) Transition between extrinsic SFs and twins; (c) Generation of the HCP structure; (d) Necking phenomenon. In Figure (d), atoms with the coordination number between 4~12 are viewed. Other figures, atoms with the *csp* value between 0.5~12 are viewed.